Ecological Indicators 150 (2023) 110230

Contents lists available at ScienceDirect

Ecological Indicators

journal homepage: www.elsevier.com/locate/ecolind

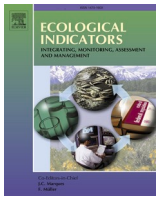

Assessment of urban flood resilience based on a systematic framework

Yuan Zhang [a,1], Wencong Yue [a,1], Meirong Su [b,a,*], Yanmin Teng [a], Qianyuan Huang [c], Weiwei Lu [d], Qiangqiang Rong [a], Chao Xu [a]

[a] Research Center for Eco-Environmental Engineering, Dongguan University of Technology, Dongguan 523808, China
[b] Key Laboratory for City Cluster Environmental Safety and Green Development of the Ministry of Education, School of Ecology, Environment and Resources, Guangdong University of Technology, Guangzhou 510006, China
[c] School of Environment, Beijing Normal University, Beijing 100875, China
[d] College of Environment and Safety Engineering, Qingdao University of Science and Technology, Qingdao 266042, China

ARTICLE INFO

Keywords:
Urban flood
Resilience
Systematic assessment framework
System performance curve
Dongguan

ABSTRACT

Urban flooding can seriously threaten urban ecological security and human life, and therefore urban flood resilience (UFR) is important for urban safety and stability. To comprehensively evaluate urban system performance during the entire process of rainfall, runoff, flooding, and drainage, we developed a systematic framework for UFR assessment covering runoff simulation, flood estimation, and resilience assessment, which broadly corresponded to the phases of resistance, adaptation, and recovery. The UFR in the phases of resistance, adaptation, and recovery was simulated and assessed using a system performance curve (SPC) and technically combining with the hybrid flood model while mainly considering the total simulation time and inundated urban proportion in SPC. Because the extent of urban flooding can be influenced by climate change and the rate of urbanization, we chose the corresponding representative factors of precipitation and infiltration rate and considered 21 simulation scenarios (seven rainfall return periods and three infiltration rates) for which UFR was quantified according to urban system performance. The effectiveness of this framework was demonstrated in application to a typical highly urbanized area (i.e., Dongguan, China). The following results were derived: (1) The inundated area under the pessimistic scenario (i.e., S19) would be nearly four times greater than that under the optimistic scenario (i.e., S3); (2) The values of UFR in Dongguan were 0.9494–0.9863, locating at the high and very high level; (3) The lowest UFR value was 0.6552 in the Shuixiang New City district; and (4) The rainfall return period was the main factor influencing UFR under relatively short rainfall return periods (i.e., S1–S9), while infiltration rate was the principal influencing factor under relatively long rainfall return periods (i.e., S10–S21). The proposed systematic framework could be applied in other cities and large-scale regions like urban agglomerations and provinces.

1. Introduction

Cities play an important role in global socioeconomic development; however, many are frequently threatened by serious natural disasters such as flooding (Guo et al., 2020; Pan et al., 2021). Consideration of the performance of cities in response to such disasters, usually termed resilience, is increasingly important for safety and stability of urban system (Campanella, 2006), and it is the main reason for the proposal of urban development goals such as resilient cities and sponge cities (Li et al., 2020; Liang et al., 2020; Ma et al., 2020; Wang et al., 2017). To improve urban flood resilience (UFR) and to reduce the various associated losses, it is urgent to systematically simulate and assess urban resilience to identify the main contributing factors (Shi et al., 2021).

The concept of resilience was first introduced in ecology by Holling (1973). Subsequently, resilience was introduced to describe the capacity of a system to resist, adapt to, and recover from a disturbance (Juan-Garcia et al., 2017). Previously, the resilience was applied in many fields such as urban drainage systems (Bertilsson et al., 2019; Meng et al., 2018), urban social-ecological systems (Chen et al., 2020; Folke, 2006; Fu et al., 2021), and community systems (Cutter et al., 2008; Faulkner et al., 2018; Rapaport et al., 2018). Although often presented with different descriptions, there were two fundamental aspects to resilience:

* Corresponding author at: School of Ecology, Environment and Resources, Guangdong University of Technology, Guangzhou 510006, China.
E-mail address: sumr@gdut.edu.cn (M. Su).
[1] Contributed equally to this work.

https://doi.org/10.1016/j.ecolind.2023.110230
Received 8 January 2023; Received in revised form 27 March 2023; Accepted 5 April 2023
Available online 14 April 2023

addressing the integrity of processes, and assessing the persistence of disturbance. The former aspect meant that the entire phases of resistance, adaptation, and recovery should be comprehensively described by investigating the state of the system before, during, and after a disturbance (Wang et al., 2012). Although many previous related studies focused on assessing urban resilience to support sustainable urban planning and design (Bocchini et al., 2013; Hu et al., 2018; Ribeiro and Gonçalves, 2019), few studies considered the state of the system after the disturbances. Therefore, there is a need for establishing a conceptual framework that integrates multiple phases for assessment of urban resilience. The latter aspect identified that the corresponding methods for measurement of resilience vary depending on the actual disturbance.

Urban flooding is one of the most common and devastating natural disasters (Hua et al., 2020; Qi et al., 2022). In recent decades, a number of cities have suffered substantial flooding events that have caused considerable damage and a large number of casualties (de Koning et al., 2019; Guo et al., 2020; Li and Bortolot, 2022). UFR has long been regarded as an important indicator of urban sustainability (Dong et al., 2017; Leandro et al., 2020). Thus, assessment of UFR is important for sustainable development (Laeni et al., 2019; Xiong et al., 2020).

Owing to its merit of assembling different phases in the same curve, one of suitable methods for UFR assessment was the system performance curve (SPC) (Zheng and Huang, 2023). The efficiency and suitability of the SPC in quantifying flood resilience were better than those of other methods (e.g., multi-criteria indices-based metrics). Also, high-resolution resilience results, obtained by the SPC, can support dynamic assessment of the ability of regional systems to cope with floods (Chen et al., 2021). Meanwhile, the results of flood simulations should be incorporated in the SPC, basically provided by hydrological models and hybrid flood models. Based on pipe network data, hydrological models (e.g., SWMM, Infoworks ICM, and CADDIES) have realized major contributions to simulation of flooding disasters using certain flood indicators (e.g., flood depth, flood volume, and inundated area) (Wang et al., 2021). Although many studies have combined the SPC with hydrological models to assess flood resilience (Chen et al., 2021; Mugume et al., 2015; Wang et al., 2019), hydrological models can hardly be applied at urban or large-scale regions owing to lack of detailed pipe network data. The hybrid flood model of surface analysis in 3D Analyst (i.e., the tool of ArcGIS) and the Soil Conservation Service Curve Number (SCS-CN) model have been applied widely to flood estimation when considering the subprocesses of rainfall, runoff, and flood (Ding et al., 2021; Mignot and Dewals, 2022; Wu et al., 2022). The spatial distribution of flood in large-scale regions can be obtained by ArcGIS software. As the recovery phase in the flooding events cannot be reflected without consideration of recovery process in the events based on the hybrid flood model, the application of this model was limited in the UFR assessment.

A conceptual framework and suitable quantitative methods that integrate multiple phases should be developed for simulation and assessment of UFR. To fill this gap, the objective of this study is to develop a systematic conceptual framework for simulating and assessing UFR based on the SPC, addressing the dynamic variation of urban performance in the phases of resistance, adaptation, and recovery under flood disturbance. Quantification of system performance in the different phases will be realized based on the hybrid flood model, in which the infiltration rate of different types of urban land will be introduced to represent the urban drainage capacity and to supplement the recovery phase after the flooding. The combination of the SPC and the hybrid flood model will enable systematic simulation and assessment of UFR, which could support the development of strategies for improving urban system performance in terms of the adaptability to and recovery from urban flooding disasters. To demonstrate the effectiveness of the proposed approach, the model will be applied in a typical city of China that has undergone rapid urbanization (i.e., Dongguan).

2. Methodology

The systematic framework for UFR assessment is shown in Fig. 1, in which the overall process of a flooding disaster (e.g., rainfall, runoff, flood, and drainage) and the corresponding phase of resilience (e.g., resistance, adaptation, and recovery) are considered. Specifically, rainfall and runoff correspond to the phase of resistance, while flood and drainage correspond to the phases of adaptation and recovery, respectively.

And the concrete technical route of UFR assessment is given in Fig. 2, in which the hybrid flood model and SPC are combined to analyze the urban flood and assess the UFR at the urban and subcatchment scale.

2.1. Runoff simulation

2.1.1. Rainfall events design

To estimate the effect of rainfall events in cities, multiple rainfall return periods (e.g., T = 1, 3, 10, 20, 50, 100, and 200 years) were designed to simulate rainfall (Wu et al., 2017). Using the rainstorm intensity formula of the Meteorological Bureau of Dongguan, rainfall intensity was calculated as follows:

$$R = \frac{3717.342 \times (1 + 0.503\lg T)}{167 \times (t_r + 14.533)^{0.729}} \tag{1}$$

where R is the designed rainfall intensity (mm/min), T is the rainfall return period (dimensionless), and the duration of rainfall t_r is set at 120 min (Wang et al., 2019).

2.1.2. Runoff simulation based on the SCS-CN model

Runoff was simulated using the SCS-CN model (NRCS, 1986), which can evaluate the impact of climate change, land use, and soil type on surface runoff under different scenarios (Xu et al., 2020). The specific calculation conducted for runoff involved Eqs. (2)–(4):

$$Q = \begin{cases} \dfrac{(P - I_a)^2}{(P - I_a + S)} & (P > I_a) \\ 0 & (P < I_a) \end{cases} \tag{2}$$

$$I_a = \lambda \times S \tag{3}$$

$$S = \frac{25400}{CN} - 254 \tag{4}$$

where Q is runoff (mm), P is total precipitation (mm), I_a is initial abstraction (mm), S is the potential maximum soil moisture retention (mm), λ is the initial abstraction coefficient (λ = 0.2 in this study), and CN is the curve number for each combination of land use and soil type, ranging from 0 to 100 (dimensionless).

The indicator CN represents runoff potential and it depends on the following three factors: antecedent moisture condition (AMC), hydrologic soil group (HSG), and land use (Xiao et al., 2011). The AMC factor consists of the following three types: AMC I (dry soil moisture), AMC II (moderate, normal, or average soil moisture condition), and AMC III (wet soil moisture). Four levels (A, B, C, and D) are proposed for HSG analysis based on the performance of infiltration. For example, HSG levels A and D represent the highest and lowest infiltration rates, respectively (Yang and Zhang, 2011). In the process of determining the CN parameter, AMC II fitted the urban-scale conditions without additional information. Cities generally had large areas of impervious surface in their soil composition; therefore, this study mainly considered AMC II and HSG level D to estimate runoff, and the corresponding CN value is shown in Table S1 of the Supplementary Material. Considering the potential for errors when the original CN value is used directly, the CN value adopted in this study was corrected on the basis of the proportions of local land use (e.g., cropland, woodland, grassland, water, built-up land, and unused land) in the subcatchments. The final CN

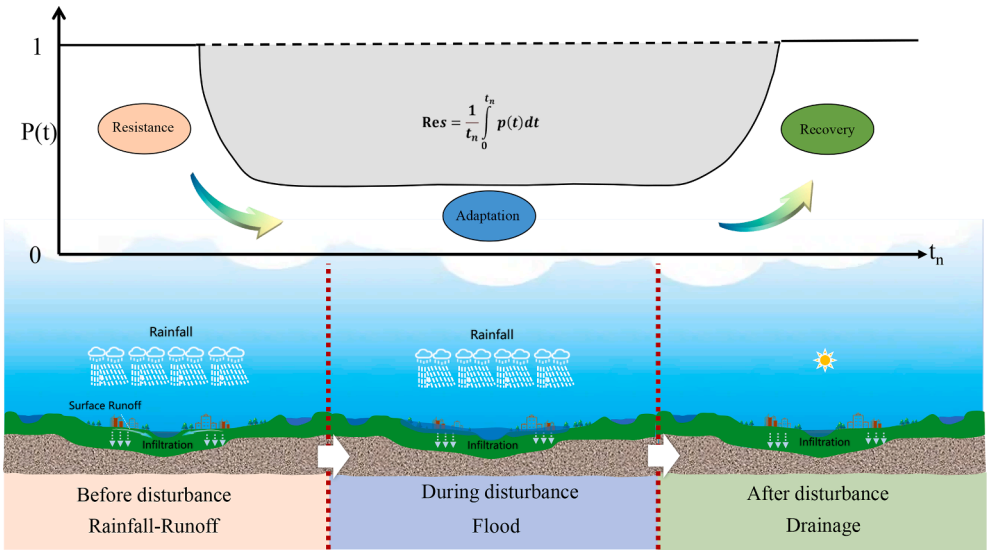

Fig. 1. Systematic framework for assessment of urban flood resilience.

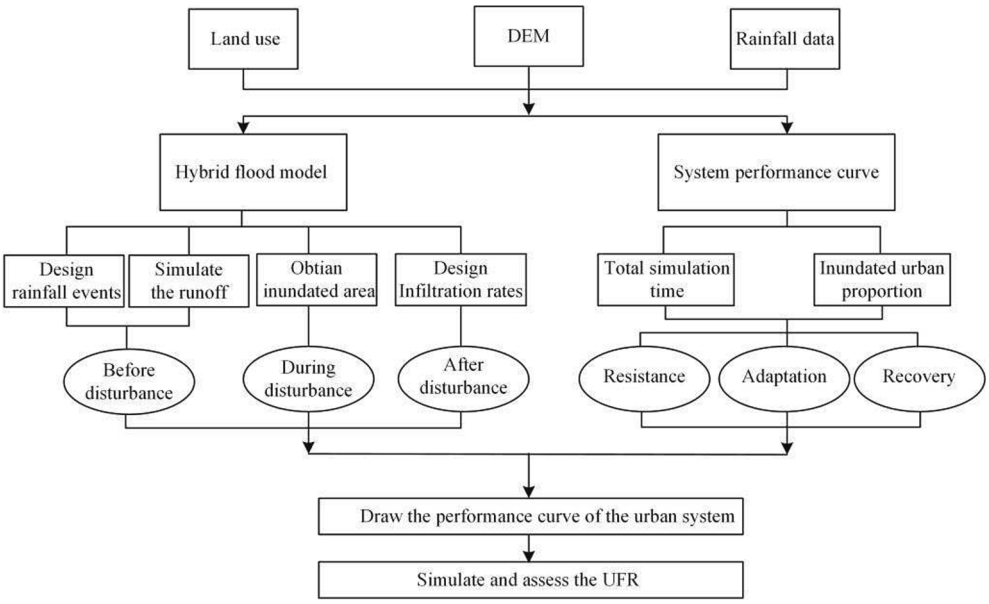

Fig. 2. Urban flood resilience assessment technological roadmap.

value of each subcatchment was obtained using the weighting method (Eq. (5)). Thus, the runoff of each subcatchment was accurately simulated when the final CN was corrected:

$$CN_n = \sum_{i=1}^{N} CN_i \times W_i \tag{5}$$

where CN_n is the final value of the n-th subcatchment, CN_i is the original value for each combination of the i-th land use types, and W_i is the percentage of the i-th land use types.

2.2. Urban flood estimation

2.2.1. Infiltration rate strategies simulation

The process of assessing UFR using the hybrid flood model needed incorporation of the recovery phase in accordance with the concept of resilience (Juan-Garcia et al., 2017). In consideration of data availability, the effects of the urban pipe network were not considered. In this study, adjustment of the infiltration rate was used to represent the urban drainage capacity. Referring to China Outdoor Drainage Design (GB50014-2021), the criteria for defining the three scenarios of infiltration rates were confirmed. The drainage capacity of mega-cities (e.g., Dongguan) in China were tend to resist the actual precipitation which would be smaller than simulated precipitation under the specific rainfall return period (e.g., T = 10). Thus, the three infiltration rate strategies ($v_{(T=1)}$, $v_{(T=3)}$, and $v_{(T=10)}$) were established based on the multiple rainfall return periods. The following steps were proposed: 1) dividing the original land use patterns into two types (i.e., built-up land and ecological land), 2) calculating the flood volume in combination with runoff by Eq. (6), and 3) evaluating the infiltration rates of the two land use types under the three short rainfall return periods using Eq. (7). It was assumed that the volume for drainage in ecological land would be equal to the flood volume under the three short rainfall return periods. Owing to the presence of some ecological land within areas of built-up land, the proportionality method was used to infer the drainage time of built-up land. Ultimately, the final infiltration rate for each

subcatchment was determined using Eq. (8):

$$V_e = \sum_{i=1}^{N} Q_i \times s_i \tag{6}$$

$$V_{ed} = s_e \times t_e \times v_e \tag{7}$$

$$v_n = \sum_{n=1}^{N} v_e \times W_{edn} + v_b \times W_{bdn} \tag{8}$$

where V_e is the flood volume of ecological land (m^3), Q_i is the runoff of the i-th land use types (mm), s_i is the area of the i-th land use types (m^2), V_{ed} is the drainage volume of ecological land (m^3), t_e is the drainage time of ecological land (min), v_e is the infiltration rate of ecological land (mm/h), v_n is the infiltration rate of the n-th subcatchment (mm/h), W_{edn} is the percentage of ecological land in the n-th subcatchment, v_b is the infiltration rate of built-up land (mm/h), and W_{bdn} is the percentage of built-up land in the n-th subcatchment.

2.2.2. Flood simulation

The final flood volume of each subcatchment (i.e., V_{fn}), calculated using Eqs. (9)-(11) after determining the runoff volume and infiltration rate, was incorporated into the surface analysis in 3D Analyst to receive the urban submerged height (Wang et al., 2021). To represent the urban flood condition and to assess UFR, the indicator of inundated area was obtained using the Raster calculator tool of ArcGIS.

$$V_n = Q_n \times s_n \tag{9}$$

$$V_{dn} = s_n \times v_n \times t_r \tag{10}$$

$$V_{fn} = V_n - V_{dn} \tag{11}$$

where V_n is the flood volume of the n-th subcatchment (m^3), Q_n is the runoff of the n-th subcatchment (mm), s_n is the area of the n-th subcatchment (m^2), V_{dn} is the drainage volume of the n-th subcatchment (m^3), and V_{fn} is the final flood volume of the n-th subcatchment (m^3).

2.3. Urban flood resilience assessment

The inundated area was chosen as a flood indicator to reflect the influence of urban flooding. UFR was calculated on the basis of the loss in system functionality and the recovery time (Bocchini et al., 2013; Hwang et al., 2015; Mugume et al., 2015). The system performance ($p(t)$) of a catchment was defined as the ratio of the number of unflooded grid cells to the total number of grid cells, as presented in Eqs. (12)-(14) (Wang et al., 2019). UFR was assessed by an aggregation of $p(t)$ during the entire simulation, as presented in Eq. (15):

$$g(i,t) = \begin{cases} 1 & d(i,t) \geqslant h_c \\ 0 & d(i,t) < h_c \end{cases} \quad where\ t \in [0, t_n] \tag{12}$$

$$N(t) = \sum_{i=1}^{N} g(i,t) \tag{13}$$

$$p(t) = 1 - \frac{N(t)}{N} \tag{14}$$

$$Res = \frac{1}{t_n} \int_0^{t_n} p(t)dt \tag{15}$$

where $d(i, t)$ is the water depth of grid cell i at time t, $g(i, t)$ is the state of grid cell i at time t, h_c is the threshold of flood depth, $N(t)$is the total number of flooded grid cells, N is the total number of grid cells in the catchment, $p(t)$ is system performance at time t, t_n is the total simulation time, and Res is the urban system resilience.

To dynamically simulate p(t) in large-scale regions, this resilience assessment model was improved on the basis of the following steps in relation to the inundation process: 1) redefining p(t) by the proportion of the unflooded area to the total area in this study by Eq. (16), 2) adopting the same 10-min interval to understand the dynamic flood condition, including the duration of rainfall and drainage time, 3) obtaining the flooded proportion using the hybrid flood model, 4) simulating the integral function of each same interval by a function fitting by Eq. (18), and 5) determining the system performance and corresponding resilience on the basis of step 4 (Fig. 3).

$$g(n,t) = \begin{cases} 1 & d(n,t) \geqslant h_{in} \\ 0 & d(n,t) < h_{in} \end{cases} \quad where\ t \in [0, t_n] \tag{16}$$

$$N(t) = \sum_{n=1}^{N} g(n,t) \tag{17}$$

$$\int_0^{t_n} p(t)dt = \sum_{j=0}^{\frac{n}{10}} \frac{(p(t_j) + p(t_{j+1})) \times t_{same}}{2} \tag{18}$$

where $d(n, t)$ is the calculated simulated height of subcatchment n at time t, h_{in} is the simulated height, $N(t)$ is the total inundated area at time t, $p(t_j)$ is the system performance at time j, $p(t_{j+1})$ is the system performance at time $j + 1$, and t_{same} is the same interval (10 min).

3. Study area

The city of Dongguan was selected for the case study to demonstrate the applicability of the proposed framework. Located in one of the fastest developing regions of China, Dongguan is strategically important to the overall development of the Pearl River Delta (Sun et al., 2018). Dongguan is a typical city that suffers urban flooding owing to the subtropical monsoon climate. Annual average temperature is 22 ℃ and mean annual precipitation is 1700 mm. In 2020, 1317 mm of precipitation was recorded during May-September (https://dgwater.dg.gov.cn/). Meanwhile, in the rapid urbanization process, the built-up area increased from 687 to 1243 km^2 during 1995–2020 (https://www.rescd.cn). Also, the rates of urbanization and built-up land in Dongguan were 92.2% and 52.2% in 2020, respectively (Rong et al., 2022).

The following data were collected in this study: (a) land use, (b) a digital elevation model, (c) an administrative map of Dongguan, and (d) delineation of the subcatchments of Dongguan based on ArcGIS (Fig. 4). The proportions of land use of each subcatchment are shown in Table S2 of the Supplementary Material. The land use and digital elevation model data were obtained from the Data Center for Resources and Environmental Science of the Chinese Academy of Sciences (https://www.rescd.cn). The administrative divisions refer to the Dongguan Agency of

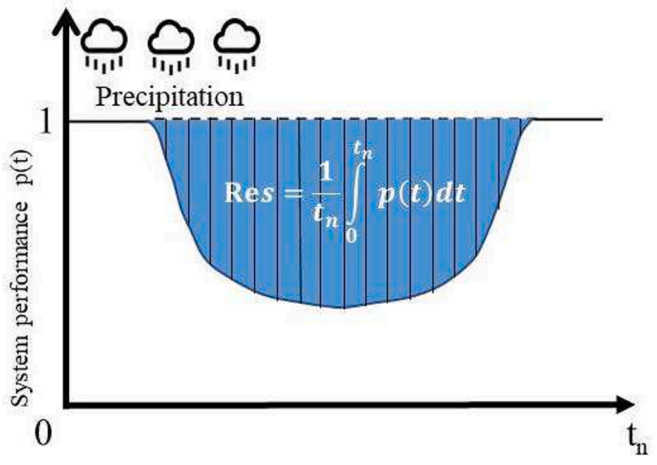

Fig. 3. System performance curve for an urban system under the precipitation.

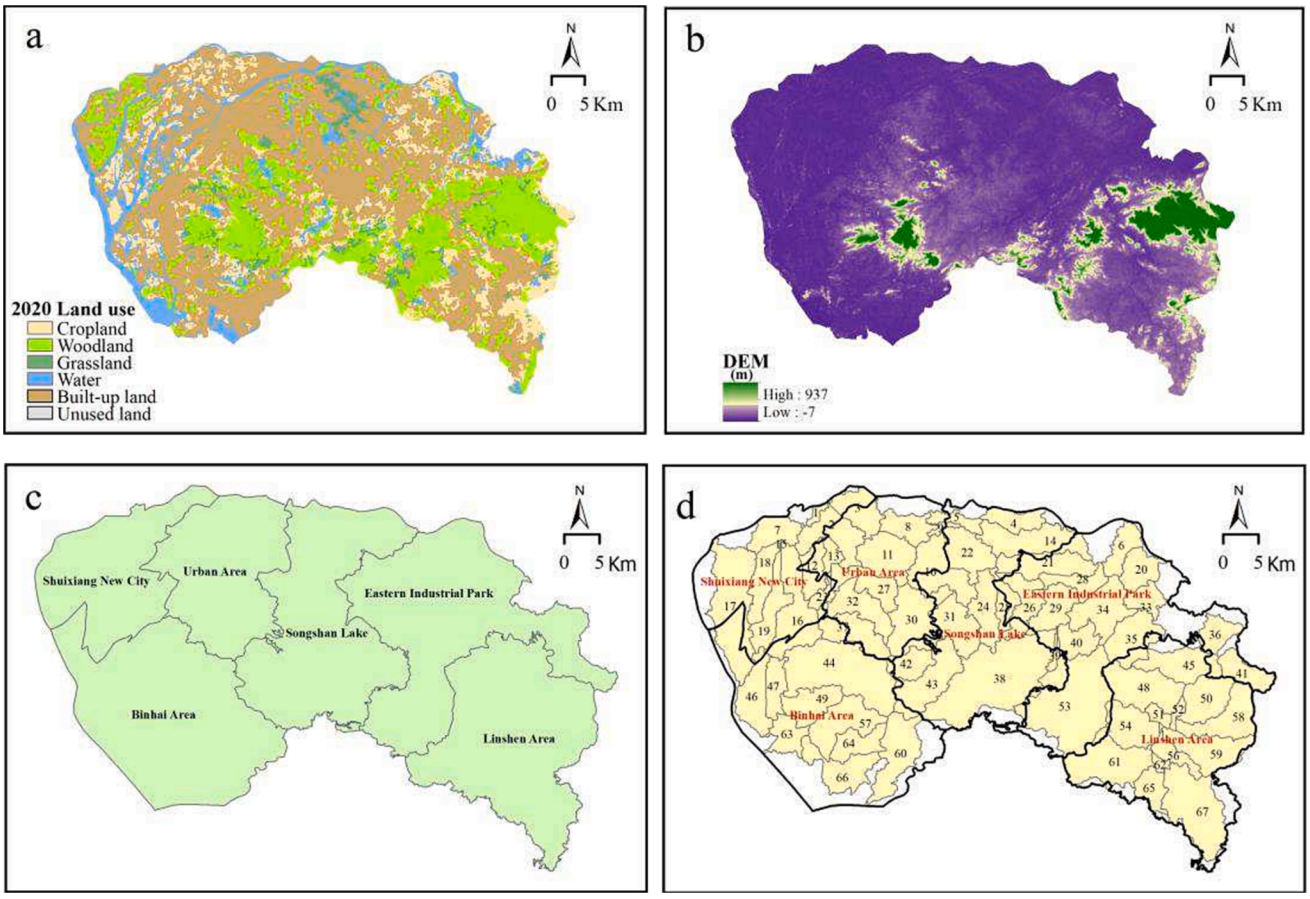

Fig. 4. (a) Land use, (b) digital elevation model, (c) administrative map, and (d) subcatchments of the city of Dongguan, China.

Natural Resources (https://nr.dg.gov.cn). It should be noted that the total subcatchment area (2164 km^2) is smaller than the Dongguan administrative area (2460 km^2).

4. Results and discussion

4.1. Runoff simulation result

Simulated using the rainstorm intensity formula (Eq. (1)), the total precipitation of Dongguan over a duration of 120 min was estimated based on multiple rainfall return periods, i.e., T = 1, 3, 10, 20, 50, 100, and 200 years, giving precipitation totals of 75, 93, 113, 124, 139, 151, and 162 mm, respectively. With reference to Wang et al. (2019), the peak of rainfall intensity occurs in the middle of the precipitation duration. As indicated in Fig. 5, the rainfall intensity was simulated to gradually increase during the first 60 min and then decrease during the second 60 min. Thus, the maximum rainfall intensity occurred at 60 min.

The infiltration rates correlated with the amount of precipitation and the proportion of underlying impervious surface. Consequently, the infiltration rate increased with increase in the proportion of ecological land. The infiltration rates associated with ecological land and built-up land are listed in Table 1. The maximum value is 36 mm/h and the minimum value is 8 mm/h, and several factors contributed to this variation. First, the infiltration rates were designed to load the pressure of rainfall. The rates were higher for the longer rainfall return periods than for other scenarios. Second, the proportion of underlying impervious surface in areas of built-up land is greater than that of ecological land. Thus, the infiltration rates of built-up land are lower than those of ecological land. The infiltration rates of the subcatchment in three scenarios are listed in Table S3 of the Supplementary Material.

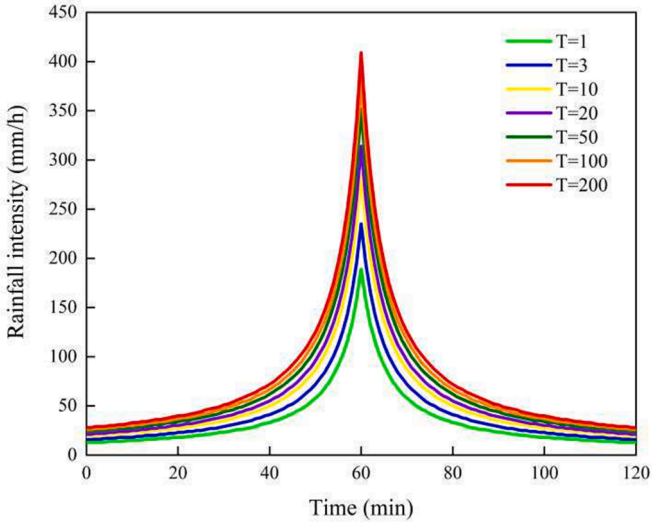

Fig. 5. Design rainfall of the seven rainfall return periods.

Table 1
Infiltration rates of land use under three strategies (mm/h).

Three strategies	Ecological land	Built-up land
$v_{(T=1)}$	20	8
$v_{(T=3)}$	27	11
$v_{(T=10)}$	36	13

4.2. Urban flood analysis

In the phase of the duration of rainfall, the indicator of inundated area was used to represent the extent of urban flooding. Generally, the extent of urban flooding is influenced by climate change and rapid urbanization (Hammond et al., 2013; Löwe et al., 2017). In this study, the extent of the inundated area depended on two factors (i.e., rainfall return period and infiltration rate). As listed in Table 2, the total inundated area increases with extension of the rainfall return period from 1 to 200 years and decreases with extension of the infiltration rate scenario from $v_{(T=1)}$ to $v_{(T=10)}$. For example, the smallest inundated area is 58.8 km^2 under S3, while the largest inundated area is 288.5 km^2 under S19. Generally, the total simulation time (i.e., duration of rainfall and drainage time) (Table 3) and the system performance directly represent the state of the flooded urban system. The smallest total time is 130 min under S3, while the largest total time is 800 min under S19.

The spatial distributions of inundated urban area under the 21 scenarios were obtained in consideration of seven rainfall return periods and three infiltration rates (Fig. 6). Generally, the main area of inundation would be located in the northwest of Dongguan (e.g., the Shuixiang New City, and Urban Area) because the infiltration rates of these areas with a high proportion of built-up land were smaller than those of others districts. Eastern parts of the Shuixiang New City district and northern parts of the Urban Area have the largest area of inundation. The regions in the north of Songshan Lake and the middle of the Eastern Industrial Park suffer a medium degree of urban flooding. Since the area proportion of ecological land (i.e., woodland and grassland) is relatively high in the Binhai Area and the Linshen Area, most parts of these two districts would suffer slight urban flooding. The specific spatial distributions of inundation in Dongguan help identify the areas prone to serious flooding and provide mitigation strategies. Ultimately, the Shuixiang New City, Urban Area, and Eastern Industrial Park districts require more attention for improvement of their UFR.

The inundated urban proportions of 2.72%–13.33% in Dongguan were smaller than that in Nanjing (7.85%–15.88%) under the rainfall return periods of T = 5–100 (Wang et al., 2021). Several factors might contribute to this difference: (1) the precipitation, which is simulated by the rainstorm intensity formula, is larger in Nanjing than in Dongguan, which means that the risk of Nanjing is higher, (2) the proportion of built-up land of Dongguan (i.e., 52.2%) is larger than that of Nanjing (i.e., 24.9 %), which means that the runoff of Dongguan is higher, and (3) the drainage capacity in Dongguan (respond to the rainfall return periods of T = 10), which is correlated with infiltration rates, is larger than that in Nanjing (respond to the rainfall return periods of T = 2), which means that the drainage capacity of Dongguan is higher.

In this study, the rainfall return periods were designed to represent extreme rainfall events. For scenarios with the same infiltration rate, longer rainfall return periods present similar areas of inundation, e.g., the inundated area is 279 and 288.5 km^2 under S16 and S19, respectively. Several factors might contribute to this phenomenon: (a) the two rainfall events reached the level of extreme heavy precipitation (i.e., more than 250 mm in under 24 h) and the total amount of precipitation in each event was similar, i.e., 151 and 162 mm, and (b) the infiltration rates ($v_{(T=1)}$) of ecological land and built-up land were 20 and 8 mm/h, respectively, which meant that the precipitation amount exceeded the drainage volume. This phenomenon was mainly reflected by the fact that the inundated area of some districts remained under the same flood condition for certain adjacent rainfall return periods. Comparison of the results for the shorter rainfall return periods reveals that the inundated areas (Table 2) varied substantially under the nine scenarios (S1–S9). The inundated area expanded when the rainfall return period and the infiltration rate both increased, e.g., 133.5 km^2 (S1), 169.9 km^2 (S5), and 192.3 km^2 (S9). This meant that the influence of precipitation is greater than that of the infiltration rate under S1–S9 in this study.

Table 2
Inundated area on the urban scale under the 21 scenarios (km^2).

	T = 1	T = 3	T = 10	T = 20	T = 50	T = 100	T = 200
$v_{(T=1)}$	133.5	192.2	223.7	250.9	266.6	279.0	288.5
$v_{(T=3)}$	81.0	169.9	204.9	226.0	256.4	266.5	282.6
$v_{(T=10)}$	58.8	125.7	192.3	204.4	227.7	260.1	263.4

Table 3
Total simulation time on the urban scale under the 21 scenarios (min).

	T = 1	T = 3	T = 10	T = 20	T = 50	T = 100	T = 200
$v_{(T=1)}$	270	380	500	570	650	730	800
$v_{(T=3)}$	170	240	330	380	450	500	550
$v_{(T=10)}$	130	180	250	290	340	390	430

4.3. Resilience assessment result

4.3.1. System performance results

In this study, the values of $p(t)$, indicated by the proportion of unflooded urban area during the total simulation time, were used to describe the state of the urban system (Fig. 7). Generally, $p(t)$ gradually declined with increasing rainfall, and it reached its minimum value for rainfall of over 120 min. The values of $p(t)$ gradually rose to 1 when the rainfall pressure disappeared and the infiltration rate reacted continuously. For the same rainfall return period, the $p(t)$ values at high infiltration rates were larger than those at low infiltration rates. The reason was that high infiltration rates represent greater drainage capacity. For the same infiltration rate, the $p(t)$ values of shorter rainfall return periods were higher than those of longer rainfall return periods. The maximum value of $p(t)$ was 0.97 under S3, while the minimum value of $p(t)$ was 0.86 under S19. Under high infiltration rates and short rainfall return periods (e.g., S3, S6, and S9), the values of $p(t)$ maintained the same level because the infiltration capacity exceeded the flood pressure during the duration of rainfall, e.g., the value of $p(t)$ was maintained at 0.97 from 70 to 120 min under S3; other scenarios also exhibited the same phenomenon.

4.3.2. UFR values on the urban scale

The UFR values of Dongguan are listed in Table 4. Influenced by the rainfall return periods and infiltration rates, UFR values are more than 0.9494 in Dongguan. Rainfall, regarded as an indicator of disturbance, has a negative impact on UFR. Infiltration rates, regarded as an indicator of recovery, has a positive impact on UFR. The UFR value declined with extension of the rainfall return periods when the infiltration rates remained unchanged. Similarly, the UFR value generally increased with improvement in the infiltration rates when the rainfall return periods remained unchanged. Thus, the UFR value was the biggest (i.e., 0.9863) under S3 and the smallest (0.9494) under S19. The UFR value will decrease if both the rainfall return period and the infiltration rate increase under S1-S9. The influence of rainfall return periods to the UFR would be more obvious than that of infiltration rate under S1 to S9. The UFR value would not decrease under S10-S21, if both the rainfall return period and the infiltration rate increase. Thus, the influence of infiltration rate to the UFR would be more obvious than that of rainfall return period under S10 to S21.

In comparison with the related studies in Xiangzhou District of Zhuhai and Siergou area in Dalian (Chen et al., 2021; Wang et al., 2019), the UFR values in Dongguan are smaller than that in Zhuhai and Dalian. These differences may be derived from the proportion of built-up land, rainfall return periods, or infiltration rates. The UFR values in 22.6% and 77.4% subcatchments in the Siergou area in Dalian were 0.60–0.90 and 0.90–1.00 under 2-h design rainfall for 200-year return period, respectively. Similarly, the UFR values in 29.8% and 70.2% subcatchments under the pessimistic scenario (i.e., S19) were 0.60–0.90 and 0.90–1.00 in this study. The UFR values is correlated with the system performance (i.e., unflood proportion) and total simulation time.

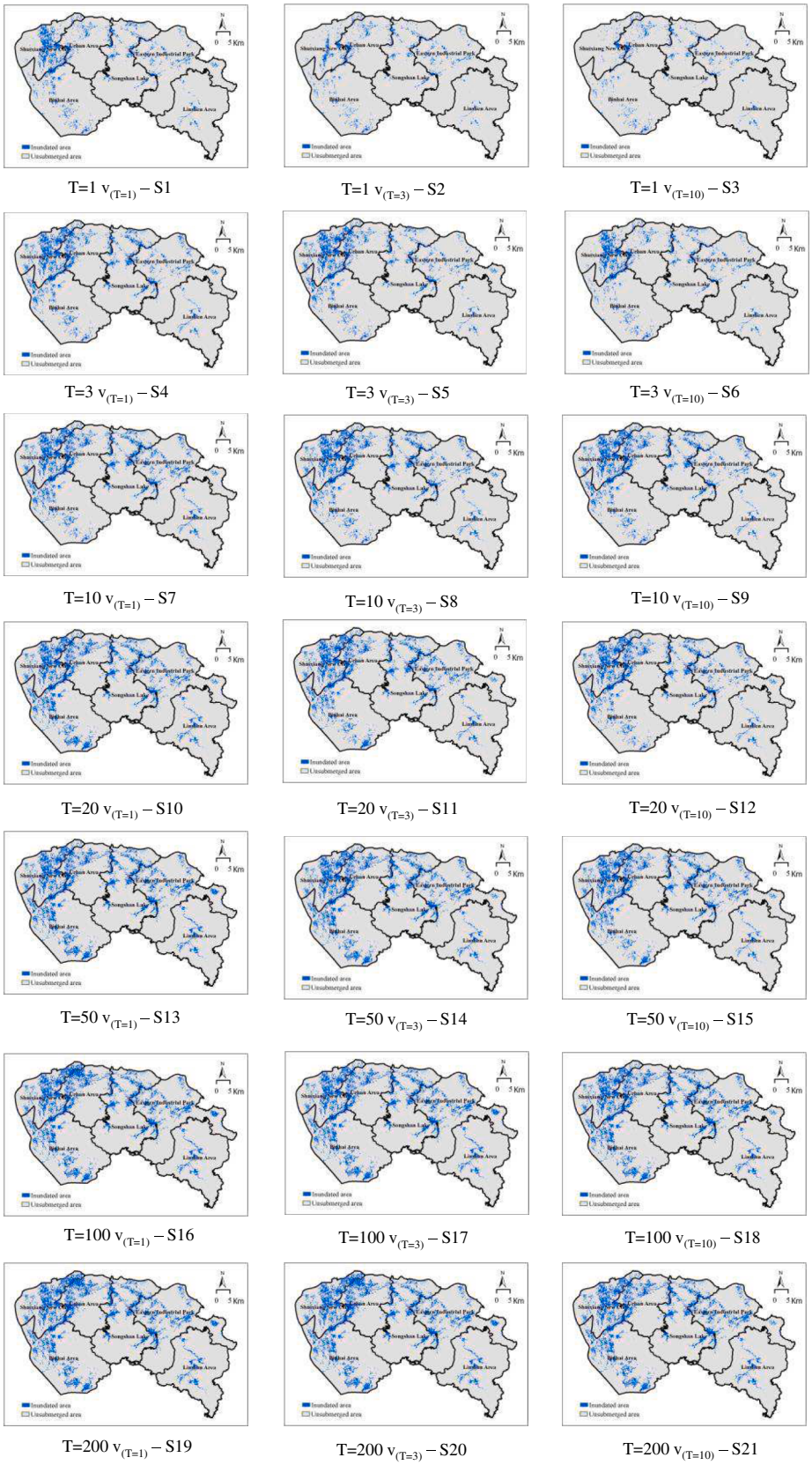

Fig. 6. Spatial distributions of inundated urban area.

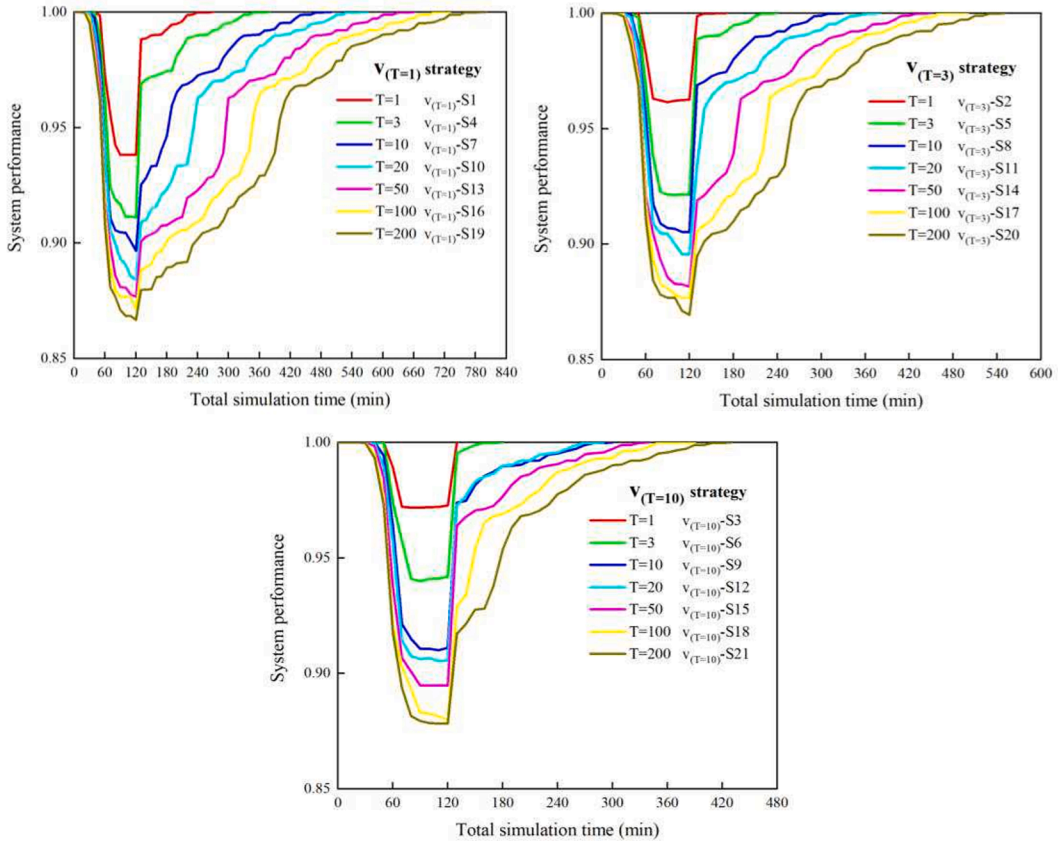

Fig. 7. Urban system performance under the 21 scenarios.

Table 4
Urban flood resilience (UFR) values under the 21 scenarios.

	T = 1	T = 3	T = 10	T = 20	T = 50	T = 100	T = 200
$v_{(T=1)}$	0.9832	0.9772	0.9701	0.9645	0.9581	0.9538	0.9494
$v_{(T=3)}$	0.9856	0.9771	0.9740	0.9711	0.9645	0.9601	0.9558
$v_{(T=10)}$	0.9863	0.9793	0.9476	0.9739	0.9712	0.9678	0.9638

Although the area of regions, and infiltration rates were different, the distributed proportions of UFR values were similar.

4.3.3. *UFR values on subcatchment scale*

The UFR values on subcatchment scale were quantified according to urban system performance. The UFR values were found similar under

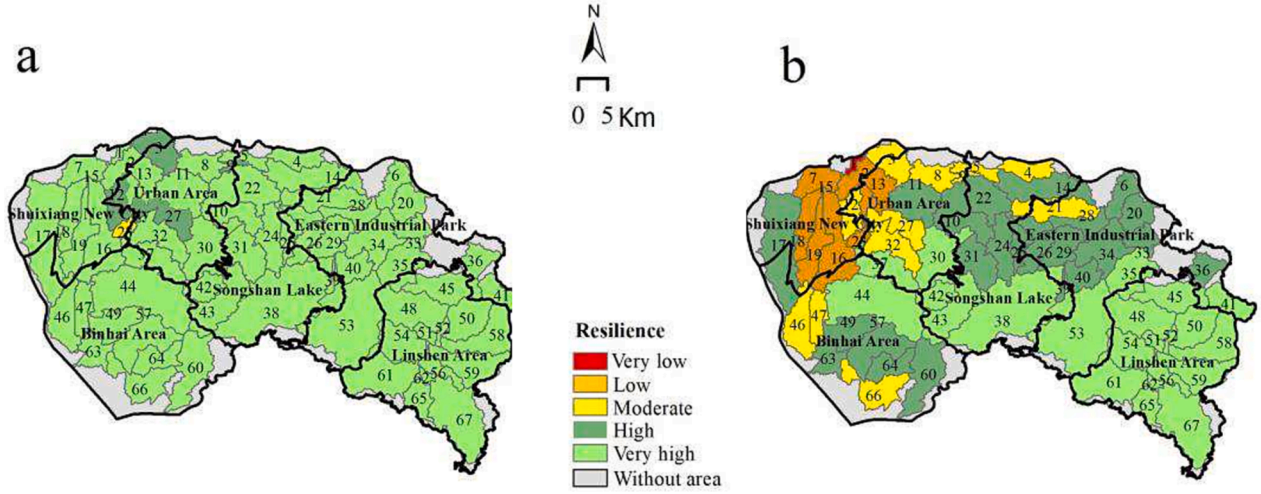

Fig. 8. Subcatchment-scale UFR under (a) S3 and (b) S19.

adjacent scenarios, being constrained by the threshold of flood depth and flood volume. Thus, an optimistic scenario S3 and a pessimistic scenario S19 were chosen to analyze the UFR values on the subcatchment scale (see Fig. 8). The UFR values were divided into five levels, i.e., very low (0.60–0.70), low (0.70–0.80), moderate (0.80–0.90), high (0.90–0.95) and very high (0.95–1.00).

In terms of the optimistic scenario (i.e., S3), UFR values in most districts would be very high (i.e., more than 0.95), indicating the ability of resisting to flood disasters. In other words, the drainage speed of urban underlying surface are bigger than the precipitation density with the high UFR values. For example, except the 23rd subcatchment in Shuixiang New City which belonged to the moderate level, the UFR values of other subcatchment fell into the high and very high levels. In terms of the pessimistic scenario (i.e., S19), the UFR values of 23 and 24 subcatchments belonged to the high and very high levels, respectively. The maximum UFR value, indicating the good performance of adapting flood, occured in Linshen Area. Conversely, the UFR values of the other subcatchments were less than 0.90. The minimum UFR value is 0.6552 in the Shuixiang New City district, indicating the very low level for adapting flood. Some strategies needed to be applied to improve the resilience of these vulnerable districts in the future. The certain districts presented some special conditions. For example, although precipitation changed substantially from S3 to S19, the UFR of the Linshen Area remained the same under the two scenarios. This means that this district had favorable capacity to adapt to flood disasters. The UFR values of all subcatchments under the 21 scenarios are listed in Table S4 of the Supplementary Material. The findings of this study could help identify urban districts vulnerable to flooding on the basis of UFR values.

5. Conclusions

Frequent flood disasters can seriously threaten the stability of urban systems. To improve the capacity of an urban system to cope with flooding, increasing attention has been paid to UFR, being critical for urban safety and stability. We suggested that systematic simulation and assessment of UFR should be vital for investigating the features of urban system and contributions of indicators in the entire process of an urban system when faced with a flood event. Correspondingly, this study developed a systematic framework for simulation and assessment of UFR, incorporating the entire processes of a flood event (e.g., rainfall, runoff, flood, and drainage) and the related phases of resilience (e.g., resistance, adaptation, and recovery). Quantification of UFR was revealed by an improved hybrid flood model and the SPC. The proposed systematic framework could be extended to simulation and assessment of resilience to flooding in cities or large-scale regions such as urban agglomerations and provinces after acquiring the essential data of simulated rainfall data, land use, digital elevation model, drainage infrastructure planning and administrative map. To verify the effectiveness of the framework, the city of Dongguan in China was selected as a case study. Twenty-one scenarios were proposed on the basis of multiple rainfall return periods and infiltration rates. The following results were obtained: (1) the inundated area of Dongguan would account for 58.8–288.5 km^2, and the recovery time would vary in the range of 10–680 min, (2) on the urban scale, system performance (i.e., unflood proportion) and UFR value would be 0.86–0.97 and 0.9494–0.9863, respectively, (3) the UFR values would increase with the growth of infiltration rate for subcatchments, and (4) indicators of rainfall return periods and infiltration rates would be the main factor influencing UFR values under relatively short rainfall return periods and relatively long rainfall return periods, respectively. On the basis of the derived results, the following policy recommendations were proposed: (1) improving the proportion of ecological land in the seriously inundated districts like Urban Area and Shuixiang New City to increase drainage capacity, or establishing some low-impact development strategies, (2) promoting draining efficiency and coverage ratio of the urban pipe network according to the contribution of urban drainage infrastructure on UFR, and (3) providing special support for the vulnerable districts (e.g., the first subcatchment) according to the UFR values.

This study had some limitations. First, the summed subcatchment area was relatively smaller than the total administrative area of Dongguan, generated by the accuracy of DEM data. Second, the values of inundated area and the UFR values were similar in adjacent scenarios, suggesting that in-depth analysis should be required to explore the underlying intrinsic principles. Third, based on the UFR values under the multiple scenarios in the current study, the strategies of improving UFR should be further focused on in the future, to support decision-making in recovering and reconstructing urban functions under the flood disturbance.

CRediT authorship contribution statement

Yuan Zhang: Conceptualization, Methodology, Formal analysis, Writing – original draft. **Wencong Yue:** Supervision, Writing – review & editing. **Meirong Su:** Conceptualization, Supervision, Funding acquisition, Writing – review & editing. **Yanmin Teng:** Investigation, Visualization. **Qianyuan Huang:** Investigation, Formal analysis. **Weiwei Lu:** Visualization, Writing – review & editing. **Qiangqiang Rong:** Investigation, Formal analysis. **Chao Xu:** Data curation, Software.

Declaration of Competing Interest

The authors declare that they have no known competing financial interests or personal relationships that could have appeared to influence the work reported in this paper.

Data availability

Data will be made available on request.

Acknowledgments

This work was supported by the National Key Research Program of China (Grant Nos. 2022YFF1301200 and 2022YFC3202200), National Science Foundation of China (No. 72122004), and Social Sciences of the Ministry of Education of China (22YJCZH228). We thank James Buxton MSc, from Liwen Bianji (Edanz) (www.liwenbianji.cn/), for editing the English text of a draft of this manuscript. The authors much appreciate the editor and the anonymous reviewers for their constructive comments and suggestion which are extremely helpful for improving the paper.

Appendix A. Supplementary data

Supplementary data to this article can be found online at https://doi.org/10.1016/j.ecolind.2023.110230.

References

Bertilsson, L., Wiklund, K., de Moura Tebaldi, I., Rezende, O.M., Veról, A.P., Miguez, M. G., 2019. Urban flood resilience – A multi-criteria index to integrate flood resilience into urban planning. J. Hydrol. 573, 970–982. https://doi.org/10.1016/j.jhydrol.2018.06.052.

Bocchini, P., Frangopol, D.M., Ummenhofer, T., Zinke, T., 2013. Resilience and Sustainability of Civil Infrastructure: Toward a Unified Approach. J. Infrastruct. Syst. 20 https://doi.org/10.1061/(asce)is.1943-555x.0000177.

Campanella, T.J., 2006. Urban Resilience and the Recovery of New Orleans. J. Am. Plann. Assoc. 72, 141–146. https://doi.org/10.1080/01944360608976734.

Chen, J., Chen, W., Huang, G., 2021. Assessing urban pluvial flood resilience based on a novel grid-based quantification method that considers human risk perceptions. J. Hydrol. 601, 126601.

Chen, C., Xu, L., Zhao, D., Xu, T., Lei, P., 2020. A new model for describing the urban resilience considering adaptability, resistance and recovery. Saf. Sci. 128, 104756.

Cutter, S.L., Barnes, L., Berry, M., Burton, C., Evans, E., Tate, E., Webb, J., 2008. A place-based model for understanding community resilience to natural disasters. Global Environ. Change-Human Policy Dimensions 18, 598–606. https://doi.org/10.1016/j.gloenvcha.2008.07.013.

Ding, S., Wang, N., Ni, L., Zeng, J., 2021. Study on the inundation risk of disaster space in the Min Delta urban agglomeration based on SCS-CN and GIS coupling model. J. Catastrophol. 37, 171–177 (in Chinese). http://doi.org/10.3969/j. issn. 1000-811X. 2022. 01. 029.
de Koning, K., Filatova, T., Need, A., Bin, O., 2019. Avoiding or mitigating flooding: Bottom-up drivers of urban resilience to climate change in the USA. Glob. Environ. Chang. 59, 101981.
Dong, X., Guo, H., Zeng, S., 2017. Enhancing future resilience in urban drainage system: Green versus grey infrastructure. Water Res. 124, 280–289. https://doi.org/10.1016/j.watres.2017.07.038.
Faulkner, L., Brown, K., Quinn, T., 2018. Analyzing community resilience as an emergent property of dynamic social-ecological systems. Ecol. Soc. 23 https://doi.org/10.5751/es-09784-230124.
Folke, C., 2006. Resilience: The emergence of a perspective for social–ecological systems analyses. Glob. Environ. Chang. 16, 253–267. https://doi.org/10.1016/j.gloenvcha.2006.04.002.
Fu, X., Hopton, M.E., Wang, X., 2021. Assessment of green infrastructure performance through an urban resilience lens. J. Clean. Prod. 289, 125146.
Guo, J., Wu, X., Wei, G., 2020. A new economic loss assessment system for urban severe rainfall and flooding disasters based on big data fusion. Environ. Res. 188, 109822 https://doi.org/10.1016/j.envres.2020.109822.
Hammond, M.J., Chen, A.S., Djordjević, S., Butler, D., Mark, O., 2013. Urban flood impact assessment: A state-of-the-art review. Urban Water J. 12, 14–29. https://doi.org/10.1080/1573062x.2013.857421.
Holling, C.S., 1973. Resilience and Stability of Ecological Systems. Annu. Rev. Ecol. Syst. 4 (1), 1–23.
Hu, M., Zhang, J., Huang, J., 2018. Assessing Social-Ecological System Resilience in Mainland China. Pol. J. Environ. Stud. 27, 1085–1096. https://doi.org/10.15244/pjoes/76242.
Hua, P., Yang, W., Qi, X., Jiang, S., Xie, J., Gu, X., Li, H., Zhang, J., Krebs, P., 2020. Evaluating the effect of urban flooding reduction strategies in response to design rainfall and low impact development. J. Clean. Prod. 242, 118515.
Hwang, H., Quintanar, D.R., Lansey, K., 2015. Resilience-based failure mode effects and criticality analysis for regional water supply system. J. Hydroinf. 17, 193–210. https://doi.org/10.2166/hydro.2014.111.
Juan-Garcia, P., Butler, D., Comas, J., Darch, G., Sweetapple, C., Thornton, A., Corominas, L., 2017. Resilience theory incorporated into urban wastewater systems management. State of the art. Water Res. 115, 149–161. https://doi.org/10.1016/j.watres.2017.02.047.
Laeni, N., van den Brink, M., Arts, J., 2019. Is Bangkok becoming more resilient to flooding? A framing analysis of Bangkok's flood resilience policy combining insights from both insiders and outsiders. Cities 90, 157–167. https://doi.org/10.1016/j.cities.2019.02.002.
Leandro, J., Chen, K.F., Wood, R.R., Ludwig, R., 2020. A scalable flood-resilience-index for measuring climate change adaptation: Munich city. Water Res. 173, 115502 https://doi.org/10.1016/j.watres.2020.115502.
Li, J., Bortolot, Z.J., 2022. Quantifying the impacts of land cover change on catchment-scale urban flooding by classifying aerial images. J. Clean. Prod. 344, 130992.
Li, G., Kou, C., Wang, Y., Yang, H., 2020. System dynamics modelling for improving urban resilience in Beijing, China. Resour. Conserv. Recycl. 161, 104954.
Liang, C., Zhang, X., Xu, J., Pan, G., Wang, Y., 2020. An integrated framework to select resilient and sustainable sponge city design schemes for robust decision making. Ecol. Ind. 119, 106810.
Löwe, R., Urich, C., Sto. Domingo, N., Mark, O., Deletic, A., Arnbjerg-Nielsen, K., 2017. Assessment of urban pluvial flood risk and efficiency of adaptation options through simulations – A new generation of urban planning tools. J. Hydrol. 550, 355–367.
Ma, Y., Jiang, Y., Swallow, S., 2020. China's sponge city development for urban water resilience and sustainability: A policy discussion. Sci. Total Environ. 729, 139078 https://doi.org/10.1016/j.scitotenv.2020.139078.
Meng, F., Fu, G., Farmani, R., Sweetapple, C., Butler, D., 2018. Topological attributes of network resilience: A study in water distribution systems. Water Res. 143, 376–386. https://doi.org/10.1016/j.watres.2018.06.048.
Mignot, E., Dewals, B., 2022. Hydraulic modelling of inland urban flooding: Recent advances. J. Hydrol. 609, 127763.
Mugume, S.N., Gomez, D.E., Fu, G., Farmani, R., Butler, D., 2015. A global analysis approach for investigating structural resilience in urban drainage systems. Water Res. 81, 15–26. https://doi.org/10.1016/j.watres.2015.05.030.
NRCS, 1986. Urban Hydrology for Small Watersheds, United States Department of Agriculture.
Pan, Y., Zhang, B., Wu, Y., Tian, Y.u., 2021. Sustainability assessment of urban ecological-economic systems based on emergy analysis: A case study in Simao, China. Ecol. Indic. 121, 107157.
Qi, W., Ma, C., Xu, H., Zhao, K., 2022. Urban flood response analysis for designed rainstorms with different characteristics based on a tracer-aided modeling simulation. J. Clean. Prod. 355, 131797.
Rapaport, C., Hornik-Lurie, T., Cohen, O., Lahad, M., Leykin, D., Aharonson-Daniel, L., 2018. The relationship between community type and community resilience. Int. J. Disaster Risk Reduct. 31, 470–477. https://doi.org/10.1016/j.ijdrr.2018.05.020.
Ribeiro, P.J.G., Gonçalves, L., 2019. Urban resilience: A conceptual framework. Sustain. Cities Soc. 50, 101625.
Rong, Q., Liu, Q., Xu, C., Yue, W., Su, M., 2022. Optimal configuration of low impact development practices for the management of urban runoff pollution under uncertainty. J. Environ. Manage. 320, 115821.
Shi, Y., Zhai, G., Xu, L., Zhou, S., Lu, Y., Liu, H., Huang, W., 2021. Assessment methods of urban system resilience: From the perspective of complex adaptive system theory. Cities 112, 103141.
Sun, J., Li, Y.P., Gao, P.P., Suo, C., Xia, B.C., 2018. Analyzing urban ecosystem variation in the City of Dongguan: A stepwise cluster modeling approach. Environ. Res. 166, 276–289. https://doi.org/10.1016/j.envres.2018.06.009.
Wang, S.-H., Huang, S.-L., Budd, W.W., 2012. Resilience analysis of the interaction of between typhoons and land use change. Landsc. Urban Plan. 106, 303–315. https://doi.org/10.1016/j.landurbplan.2012.04.002.
Wang, P., Li, Y., Yu, P., Zhang, Y., 2021. The analysis of urban flood risk propagation based on the modified susceptible infected recovered model. J. Hydrol. 603, 127121.
Wang, Y., Sun, M., Song, B., 2017. Public perceptions of and willingness to pay for sponge city initiatives in China. Resour. Conserv. Recycl. 122, 11–20. https://doi.org/10.1016/j.resconrec.2017.02.002.
Wang, Y., Meng, F., Liu, H., Zhang, C., Fu, G., 2019. Assessing catchment scale flood resilience of urban areas using a grid cell based metric. Water Res. 163, 114852 https://doi.org/10.1016/j.watres.2019.114852.
Wu, X., Wang, Z., Guo, S., Liao, W., Zeng, Z., Chen, X., 2017. Scenario-based projections of future urban inundation within a coupled hydrodynamic model framework: A case study in Dongguan City, China. J. Hydrol. 547, 428–442. https://doi.org/10.1016/j.jhydrol.2017.02.020.
Wu, Z., Xue, W., Xu, H., Yan, D., Wang, H., Qi, W., 2022. Urban Flood Risk Assessment in Zhengzhou, China, Based on a D-Number-Improved Analytic Hierarchy Process and a Self-Organizing Map Algorithm. Remote Sens. (Basel) 14 (19), 4777.
Xiao, B., Wang, Q.-H., Fan, J., Han, F.-P., Dai, Q.-H., 2011. Application of the SCS-CN Model to Runoff Estimation in a Small Watershed with High Spatial Heterogeneity. Pedosphere 21, 738–749. https://doi.org/10.1016/s1002-0160(11)60177-x.
Xiong, F., Guo, S., Yin, J., Tian, J., Rizwan, M., 2020. Comparative study of flood regional composition methods for design flood estimation in cascade reservoir system. J. Hydrol. 590, 125530.
Xu, C., Rahman, M., Haase, D., Wu, Y., Su, M., Pauleit, S., 2020. Surface runoff in urban areas: The role of residential cover and urban growth form. J. Clean. Prod. 262, 121421.
Yang, J.-L., Zhang, G.-L., 2011. Water infiltration in urban soils and its effects on the quantity and quality of runoff. J. Soil. Sediment. 11, 751–761. https://doi.org/10.1007/s11368-011-0356-1.
Zheng, J., Huang, G., 2023. A novel grid cell-based urban flood resilience metric considering water velocity and duration of system performance being impacted. J. Hydrol. 617, 128911.